Astronomical Journal
Preprint typeset using LATEX style emulateapj v. 11/26/04

arXiv:astro-ph/0602143v2 10 Feb 2006

INFRARED 3–4 μM SPECTROSCOPY OF INFRARED LUMINOUS GALAXIES WITH POSSIBLE SIGNATURES OF OBSCURED ACTIVE GALACTIC NUCLEI

Masatoshi Imanishi[1,2,3]
National Astronomical Observatory, 2-21-1, Osawa, Mitaka, Tokyo 181-8588, Japan
Astronomical Journal

ABSTRACT

We present the results of infrared 2.8–4.1 μm (*L*-band) spectroscopy of nearby infrared luminous galaxies with possible signatures of dust-obscured active galactic nuclei (AGNs) in data at other wavelengths. The samples are chosen to include sources with a radio excess relative to far-infrared emission, strong absorption features in mid-infrared 5–11.5 μm spectra, unusually weak [CII] 158 μm emission relative to the far-infrared continuum, and radio galaxies classified optically as narrow-line objects. Our aim is to investigate whether the signatures of possible obscured AGNs can be detected in our *L*-band spectra, based on the strengths of emission and absorption features. Six of nine observed sources clearly show 3.3 μm polycyclic aromatic hydrocarbon (PAH) emission features, a good starburst indicator. An absorption feature at 3.1 μm due to ice-covered dust is detected in IRAS 04154+1755 and IRAS 17208−0014. The signature of a bare carbonaceous dust absorption feature at 3.4 μm is seen in NGC 1377. Our *L*-band spectra reveal strong signatures of obscured AGNs in all three optical Seyfert 2 galaxies (IRAS 04154+1755, Cygnus A, and 3C 234), and two galaxies classified optically as non-Seyferts (NGC 828 and NGC 1377). Among the remaining optical non-Seyferts, IRAS 17208−0014 might also show a buried AGN signature, whereas no explicit AGN evidence is seen in the *L*-band spectra of the mid-infrared absorption-feature source IRAS 15250+3609, and two weak [CII] emitters IC 860 and CGCG 1510.8+0725.

Subject headings: galaxies: active — galaxies: ISM — galaxies: nuclei — galaxies: Seyfert — galaxies: starburst — infrared: galaxies — galaxies: individual: IRAS 04154+1755, NGC 828, IRAS 15250+3609, IRAS 17208−0014, NGC 1377, IC 860, CGCG 1510.8+0725, Cygnus A, 3C 234

1. INTRODUCTION

Infrared luminous galaxies ($L_{IR} \gtrsim 10^{11} L_\odot$) radiate most of their luminosity as dust emission in the infrared (Sanders & Mirabel 1996). Thus, powerful energy sources, e.g., starbursts and/or active galactic nuclei (AGNs), must be present hidden behind dust. In the local universe, these infrared luminous galaxies dominate the bright end of the luminosity function (Soifer et al. 1987). In the distant universe, they dominate the cosmic infrared background emission and have been used to trace the dust-obscured star-formation rate, dust content, and metallicity in the early universe, based on the assumption that they are powered by starbursts (Barger et al. 2000). Estimating the AGN contribution to their infrared luminosities is therefore important, not only to obtain a full understanding of the nature of these galaxies, but also to study the connections between obscured AGNs and starbursts in the universe.

In a powerful AGN that is obscured along our sightline by dust in a *torus* geometry, the hard radiation of AGN can photo-ionize clouds along the torus axis, above the torus scale height, and can produce the so-called narrow line regions (NLRs; Antonucci 1993; Robson 1996). Since the NLRs show optical spectra that differ from normal star-forming galaxies, such obscured AGNs should be detectable through optical spectroscopy (classified as Seyfert 2s; Veilleux & Osterbrock 1987). However, since the nuclear regions of infrared luminous galaxies are very dusty (Sanders & Mirabel 1996), virtually all lines of sight can be opaque to the bulk of the ionizing radiation of AGNs. In such *buried* AGNs [4], X-ray dissociation regions (XDRs), which are dominated by low-ionization species (Maloney et al. 1996), develop instead of the NLRs, so that it is difficult to find AGN signatures using either conventional optical spectroscopy or high-resolution infrared spectroscopic searches for high-excitation forbidden emission lines that originate in the NLRs (Genzel et al. 1998; Veilleux et al. 1999; Murphy et al. 2001). From the spectral shape of the cosmic X-ray background emission, it is inferred that buried AGNs are abundant in the universe (Fabian et al. 2002); therefore, establishing a method with which to detect such optically elusive (Maiolino et al. 2003) buried AGNs is very important.

To find such buried AGNs, it is necessary to conduct observations at wavelengths with low dust extinction. Infrared *L*-band (2.8–4.1 μm) spectroscopy from the ground is one of the most powerful tools for this purpose. First, dust extinction in the *L*-band is lower than at shorter wavelengths ($A_L \sim 0.06 \times A_V$; Rieke & Lebofsky 1985) and is as low as at 5–13 μm (Lutz et al. 1996).

Electronic address: masa.imanishi@nao.ac.jp

[1] Based in part on data collected at Subaru Telescope, which is operated by the National Astronomical Observatory of Japan.

[2] Visiting Astronomer at the Infrared Telescope Facility, which is operated by the University of Hawaii under Cooperative Agreement no. NCC 5-538 with the National Aeronautics and Space Administration, Office of Space Science, Planetary Astronomy Program.

[3] Department of Astronomy, School of Science, Graduate University for Advanced Studies, Mitaka, Tokyo 181-8588

[4] We use the term "obscured AGN" if the AGN is obscured along our line of sight, and "buried AGN" if the AGN is obscured along virtually all sightlines.

Second, the contribution from AGN-powered dust emission to an observed flux, relative to stellar emission, increases substantially compared to $\lambda < 2$ μm. Therefore, the detection of buried AGNs becomes more feasible than at $\lambda < 2$ μm. Third, emission from a normal starburst and AGN are clearly distinguishable based on *L*-band spectra (Moorwood 1986; Imanishi & Dudley 2000). A strong polycyclic aromatic hydrocarbon (PAH) emission feature is usually found at 3.3 μm in a normal starburst galaxy (Moorwood 1986). In a pure normal starburst, high equivalent-width 3.3 μm PAH emission ($\mathrm{EW_{3.3PAH}}$ $\sim$ 100 nm; Moorwood 1986; Imanishi & Dudley 2000) should always be found, since the equivalent width is, by definition, insensitive to dust extinction of the starburst. In a pure AGN, PAH molecules are destroyed, rather than excited, by X-ray radiation of the AGN (Voit 1992; Siebenmorgen et al. 2004), so that no 3.3 μm PAH emission is expected (Moorwood 1986). Instead, a featureless continuum from submicron-sized (Draine & Lee 1984; Mathis & Whiffen 1989) hot dust heated by an AGN is found, making a PAH-free smooth 3–4 μm spectrum. In an AGN/starburst composite galaxy, 3.3 μm PAH emission from the starburst should be found, unless the starburst regions are directly exposed to the X-ray radiation of the AGN; however, the PAH emission is strongly diluted by the AGN-originating PAH-free continuum, so the $\mathrm{EW_{3.3PAH}}$ value should be reduced compared to a pure normal starburst galaxy. Thus, the presence of an obscured AGN can be established using the $\mathrm{EW_{3.3PAH}}$ value.

If a highly dust-obscured AGN is present, and yet the AGN emission contributes significantly to the observed *L*-band flux, then absorption features at 3.1 and 3.4 μm produced by ice-covered dust and bare carbonaceous dust, respectively, should be found (Imanishi & Dudley 2000; Imanishi & Maloney 2003; Risaliti et al. 2003, 2006; Imanishi et al. 2006). Although a normal starburst, in which stellar energy sources and dust are spatially well mixed (Puxley 1991; McLeod et al. 1993; Forster Schreiber et al. 2001), can also show these absorption features (Sturm et al. 2000), there is an upper limit for the absorption optical depths (Imanishi & Maloney 2003; Imanishi et al. 2006). This is because in this mixed source/dust geometry, the less-obscured, less-attenuated emission from the foreground (which shows weak dust absorption features) makes a stronger contribution to the observed flux than the emission from the distant side (which shows strong dust absorption features but is highly attenuated). Thus, strong dust absorption features whose optical depths are larger than the upper limit determined by the mixed source/dust geometry indicate that obscuring dust is present as a foreground screen distribution (Imanishi & Maloney 2003; Imanishi et al. 2006). A compact energy source that is more centrally concentrated than the surrounding dust, such as a buried AGN, is a natural explanation (Imanishi & Maloney 2003; Imanishi et al. 2006), unless a large amount of dust in a nearly edge-on host galaxy is present in front of the primary 3–4 μm continuum-emitting energy source.

Imanishi et al. (2006) presented *L*-band spectra of a large number of nearby ultraluminous infrared galaxies ($\mathrm{L_{IR}} > 10^{12}\mathrm{L_\odot}$; Sanders & Mirabel 1996) in the well-studied *IRAS* 1 Jy sample (Kim & Sanders 1998), searched for possible signatures of powerful buried AGNs in these galaxies, and statistically investigated the properties of buried AGNs. However, there also exist several ultraluminous infrared galaxies ($\mathrm{L_{IR}} > 10^{12}\mathrm{L_\odot}$) not included in the *IRAS* 1 Jy sample, as well as galaxies with $\mathrm{L_{IR}} < 10^{12}\mathrm{L_\odot}$, that show possible signatures of AGNs obscured behind dust in data at other wavelengths. In this paper, we present ground-based *L*-band spectra of such galaxies, with the aim of testing if this *L*-band spectroscopic method is indeed effective at finding AGN signatures. Throughout this paper, $H_0 = 75$ km s^{-1} Mpc^{-1}, $\Omega_\mathrm{M} = 0.3$, and $\Omega_\Lambda = 0.7$ are adopted.

2. TARGETS

Infrared luminous galaxies that have the following properties were observed. (1) They do not belong to ultraluminous infrared galaxies in the *IRAS* 1 Jy sample and thus were not presented by Imanishi et al. (2006). (2) Observations at other wavelengths have indicated at least some signatures of obscured AGNs. (3) No high-quality *L*-band spectra were published in the literature at the time of our observations. Table 1 summarizes the observed targets. The sample selection is heterogeneous, but our *L*-band spectra can provide useful information about the nature of these interesting galaxies.

2.1. *Radio excess relative to far-infrared emission*

In normal starburst galaxies, the radio and far-infrared luminosities are correlated, with a relatively small scatter (Condon et al. 1991). If a galaxy shows a significant radio excess above this correlation, then the presence of a radio-intermediate (or radio-loud) AGN is suggested. Crawford et al. (1996) investigated the radio to far-infrared luminosity ratios of ultraluminous infrared galaxies and found that IRAS 04154+1755 shows (1) the largest radio excess and (2) a jet-like radio structure. This object is classified optically as a Seyfert 2 (Crawford et al. 1996), so that a powerful radio-intermediate AGN must be present, hidden behind torus-shaped dust. No significant 2–10 keV X-ray emission from the putative AGN was detected (Imanishi & Ueno 1999), which suggests that the AGN suffers from Compton-thick ($\mathrm{N_H} > 10^{24}$ cm^{-1}) X-ray absorption.

2.2. *Strong ice absorption in mid-infrared 5–11.5 μm spectra*

Mid-infrared 5–11.5 μm spectra of many infrared luminous galaxies were taken with *ISO*. From these spectra, Spoon et al. (2002) selected 18 sources that show strong ice absorption features at 6.0 μm (their Table 1, excluding NGC 253 and M82). To detect ice absorption, a significant quantity of dust grains covered with an ice mantle must be present in the foreground of the continuum-emitting source(s). Such ice-covered dust grains are usually found deep inside molecular gas, where dust is sufficiently shielded from ambient UV radiation (Whittet et al. 1988). A normal starburst galaxy with mixed source/dust geometry can produce ice absorption features, if a sufficient quantity of ice-covered dust is present. An obscured AGN is an alternative candidate, particularly for sources with strong absorption and weak PAH emission features (see §1).

In the 5–11.5 μm spectra, PAH emission features are found at 6.2, 7.7, and 8.6 μm. In addition to the H_2O ice absorption at 6.0 μm, there are also absorption features due to hydrogenated amorphous carbon (HAC) at 6.85 and 7.3 μm, and due to silicate dust at 9.7 μm. Since these emission and absorption features overlap significantly in wavelength, it is often difficult to distinguish whether these galaxies are absorption-dominated (obscured AGN candidates) or PAH-emission-dominated (normal starbursts) (Spoon et al. 2002). L-band spectroscopy may help to distinguish whether the sources are dominated by PAH emission or absorption features (Imanishi 2000a,b; Imanishi & Dudley 2000).

Among the 18 strong ice absorption sources, eight (IRAS 00188−0856, IRAS 05189−2524, UGC 5101, NGC 4418, Mrk 231, NGC 4945, Mrk 273, Arp 220) have available high quality L-band spectra (Spoon et al. 2000; Imanishi & Dudley 2000; Imanishi et al. 2001; Imanishi & Maloney 2003; Imanishi et al. 2004, 2006). Of these eight sources, L-band spectra of five sources display signatures of obscured AGNs (IRAS 00188−0856, IRAS 05189−2524, UGC 5101, Mrk 231, and Mrk 273) (Imanishi & Dudley 2000; Imanishi et al. 2001; Imanishi & Maloney 2003; Imanishi et al. 2006), suggesting that this sample contains many obscured AGNs. For the remaining ten unobserved sources, we exclude four southern sources with declinations $< -30°$ from our target list, because they are difficult to observe from Mauna Kea, Hawaii, our main observation site. Of the remaining six sources, we observed NGC 828, IRAS 15250+3609, and IRAS 17208−0014, of which IRAS 15250+3609 shows the strongest absorption and weakest PAH emission features, making this source the strongest obscured AGN candidate. In addition, NGC 1377 (IRAS 03344−2103) is also included, because its mid-infrared spectrum (Laureijs et al. 2000) is interpreted as dominated by strong 9.7 μm silicate dust absorption ($\tau_{9.7} >$ 3.5), with weak PAH emission (Spoon et al. 2004).

2.3. *Weak [CII] 158 μm emission relative to the far-infrared continuum*

Malhotra et al. (1997) measured the [CII] 158 μm emission lines of 30 optically normal (non-Seyfert) star-forming galaxies, and found that three sources, NGC 4418, IC 860, and CGCG 1510.8+0725, show a significant [CII] deficiency relative to their far-infrared continuum luminosities. The presence of buried AGNs is a possible explanation for the [CII] deficiency (Malhotra et al. 1997), although alternative scenarios have also been proposed (Malhotra et al. 1997, 2001). In fact, detailed infrared spectroscopic studies of NGC 4418 have provided many pieces of evidence for a powerful buried AGN (Dudley & Wynn-Williams 1997; Spoon et al. 2001; Imanishi et al. 2004). For this reason, IC 860 and CGCG 1510.8+0725 are also included as targets, in the expectation that they may be objects similar to NGC 4418.

2.4. *Narrow-line radio galaxies*

Narrow-line radio galaxies show Seyfert-2-type optical spectra. According to the AGN unification paradigm, these galaxies are taken to contain powerful radio-loud AGNs hidden behind torus-geometry dust (Urry & Padovani 1995). It is of interest to investigate whether our L-band spectroscopic method can indeed successfully detect clear signatures of obscured AGNs in these galaxies that are already known to possess obscured AGNs. Two nearby narrow-line radio galaxies, Cygnus A and 3C 234, are selected.

Cygnus A is a nearby well-studied narrow-line radio galaxy (Osterbrock & Miller 1975). Strong, but moderately absorbed, power-law X-ray emission was detected (Ueno et al. 1994; Young et al. 2002), suggesting the presence of an obscured AGN. Near-infrared (1–4 μm) observations also suggested the presence of a powerful obscured AGN (A_V = 40–150 mag) (Djorgovski et al. 1994; Ward 1996; Packham et al. 1998; Tadhunter et al. 1999). Based on a mid-infrared 8–13 μm spectrum, Imanishi & Ueno (2000) suggested that the energy source is more centrally concentrated than the nuclear obscuring dust, as is expected for an obscured AGN.

3C 234 shows a broad Hα emission line in its optical spectrum (Grandi & Osterbrock 1978). However, Antonucci & Barvainis (1990) and Young et al. (1998) argued that the broad component is interpreted as a scattered component, rather than a directly transmitted component, and that optical classification of this galaxy as a narrow-line radio galaxy is more appropriate. The dust extinction toward the AGN is estimated to be A_V = 60 mag (Young et al. 1998). Sambruna et al. (1999) detected intrinsically luminous, moderately absorbed X-ray emission from the putative AGN.

3. OBSERVATIONS AND DATA ANALYSIS

Infrared L-band spectroscopic observations were made using infrared spectrographs, IRCS (Kobayashi et al. 2000) on the Subaru 8.2-m telescope (Iye et al. 2004) and SpeX (Rayner et al. 2003) on the IRTF 3-m telescope. Table 2 summarizes a detailed observation log.

For Subaru IRCS observation runs, the sky was clear during the observations and seeing sizes at $\lambda = 2.2$ μm were measured to be $0''.5$–$0''.8$ in full-width at half maximum (FWHM). A $0''.9$-wide slit and the L-grism were used with a 58-mas pixel scale. The achievable spectral resolution was ∼140 at 3.5 μm. The position angle of the slit was set along the north-south direction. A standard telescope nodding technique (ABBA pattern) with a throw of 7 arcsec along the slit was employed to subtract background emission. Each exposure was 1.5–2.0 sec, and 30–40 coadds were made at each position.

For the IRTF SpeX observations, we employed the 1.9–4.2 μm cross-dispersed mode with a $1''.6$ wide slit. This mode enables L- (2.8–4.1 μm) and K-band (2–2.5 μm) spectra to be obtained simultaneously, with a spectral resolution of R ∼ 500. The sky conditions were clear throughout the observations, and seeing sizes at $\lambda = 2.2$ μm were in the range $0''.4$–$1''.0$ FWHM. The position angle of the slit was set along the north-south direction. A standard telescope nodding technique with a throw of 7.5 arcsec was employed along the slit. The telescope tracking was monitored with the infrared slit-viewer of SpeX. Each exposure was 15 sec, and 2 coadds were made at each position.

A-, F-, and G-type main sequence stars (Table 2) were observed as standard stars, with airmass differences of <0.1 to the individual target objects, to correct for the transmission of the Earth's atmosphere. The K- and L-band magnitudes of the standard stars were estimated from their V-band (0.6 μm) magnitudes, adopting the $V-K$ and $V-L$ colors appropriate to the stellar types of individual standard stars, respectively (Tokunaga 2000).

Standard data analysis procedures were employed, using the Image Reduction and Analysis Facility (IRAF) [5]. Initially, frames taken with an A (or B) beam were subtracted from frames taken subsequently with a B (or A) beam, and the resulting subtracted frames were added and divided by a spectroscopic flat frame. Bad pixels and pixels hit by cosmic rays were then replaced with the interpolated values from surrounding pixels. Corrections for cosmic ray hits were much larger for IRTF SpeX than Subaru IRCS. Finally, the spectra of the target objects and standard stars were extracted. Wavelength calibration was performed taking into account the wavelength-dependent transmission of the Earth's atmosphere. The spectra of the targets were divided by the observed spectra of standard stars, multiplied by the spectra of blackbodies with temperatures appropriate to the individual standard stars (Table 2), and then flux-calibrated. Appropriate binning of spectral elements was performed to achieve an adequate signal-to-noise ratio ($\gtrsim$10) in most of the elements, particularly at $\lambda_{\rm obs} < 3.3$ μm in the observed frame, where the Earth's atmospheric transmission is poorer than at longer L-band wavelengths. For all sources, whole spectral datasets were divided into a few sub-groups, and error bars at each spectral element were estimated from the scatter of actual signals among the sub-groups.

4. RESULTS

4.1. *L-band spectra*

4.1.1. *3.3 μm PAH emission*

Figure 1 shows flux-calibrated nuclear L-band spectra of the nine observed sources. All sources, except NGC 1377, Cygnus A, and 3C 234, show clear emission features at $\lambda_{\rm obs} \sim (1 + z) \times 3.3$ μm, which we identify as the 3.3 μm PAH emission. The detection of the 3.3 μm PAH emission, an indicator of starbursts, means that these galaxies contain detectable starburst activity. To estimate the 3.3 μm PAH flux, we adopt a template spectral shape for Galactic star-forming regions and nearby starburst galaxies (type-1 sources; Tokunaga et al. 1991). In this template, the main 3.3 μm PAH emission profile extends between $\lambda_{\rm rest}$ = 3.24–3.35 μm in the rest frame. Data points at wavelengths slightly shorter than $\lambda_{\rm rest}$ = 3.24 μm and slightly longer than $\lambda_{\rm rest}$ = 3.35 μm, unaffected by obvious absorption features, are adopted as the continuum levels, which are shown as solid lines for PAH-detected sources in Figure 1. For sources with clearly detectable PAH emission, this template profile reproduces the observed 3.3 μm PAH emission features reasonably well, with our spectral resolution and signal-to-noise ratios, except NGC 828 which displays a slightly broader profile than the template (Figure 1, dotted lines). Table 3 summarizes the observed properties of the 3.3 μm PAH emission features. The uncertainties of the 3.3 μm PAH fluxes, estimated from the fittings, are <20% in all cases. Possible systematic uncertainties coming from continuum determination ambiguities are also unlikely to exceed 20%, as long as reasonable continuum levels are adopted. Thus, total uncertainties of the PAH fluxes are taken as <30%. Cygnus A, 3C 234, and NGC 1377 may also show excesses at the expected wavelength of 3.3 μm PAH emission, but their significance is marginal; we therefore estimate upper limits for the PAH fluxes.

4.1.2. *3.1 μm H_2O ice absorption*

IRAS 04154+1755 ($z = 0.056$) shows a concave continuum, which is naturally explained by the strong, broad 3.1 μm H_2O ice absorption feature (Spoon et al. 2000; Imanishi & Maloney 2003; Imanishi et al. 2006). The detection of this ice absorption feature means that the L-band continuum-emitting energy source is obscured by ice-covered dust grains deep inside molecular gas (Whittet et al. 1988). Following Imanishi et al. (2006), we adopt a linear continuum to estimate the optical depth of this 3.1 μm H_2O ice absorption ($\tau_{3.1}$). The continuum level varies slightly depending on the adopted data points used for the continuum determination. We adopt a relatively low continuum level to obtain a conservative lower limit for the $\tau_{3.1}$ value in IRAS 04154+1755. It is $\tau_{3.1} \sim 0.9$, which corresponds to $A_V \sim 15$ mag if the Galactic $\tau_{3.1}/A_V$ ratio ($\sim$0.06; Smith et al. 1993; Tanaka et al. 1990; Murakawa et al. 2000) is assumed. The ice absorption feature of IRAS 04154+1755 has a strong absorption wing at $\lambda_{\rm obs}$ = 3.6–3.9 μm or $\lambda_{\rm rest}$ = 3.4–3.7 μm, which resembles the absorption profile of GL 2591 (a Galactic protostar surrounded by circumstellar material), rather than Elias 16 (a Galactic late-type field star behind molecular clouds) (Smith et al. 1989).

The continuum of IRAS 17208−0014 ($z = 0.042$) is also concave-shaped. We obtain $\tau_{3.1} \sim 0.4$, which is similar to the recent estimate by Risaliti et al. (2006), using independent data. Unlike IRAS 04154+1755, the ice absorption feature of IRAS 17208−0014 has a relatively weak absorption wing at $\lambda_{\rm obs}$ = 3.55–3.85 μm or $\lambda_{\rm rest}$ = 3.4–3.7 μm, as seen in Elias 16, rather than GL 2591 (Smith et al. 1989).

4.1.3. *3.4 μm bare carbonaceous dust absorption*

NGC 1377 (z = 0.005) shows an absorption feature that peaks at $\lambda_{\rm obs}$ = 3.4–3.45 μm, or $\lambda_{\rm rest} \sim 3.4$ μm. We interpret this to be the 3.4 μm dust absorption feature produced by bare carbonaceous dust grains, which is found in Galactic stars highly reddened by the *diffuse* interstellar medium outside molecular gas (Pendleton et al. 1994; Imanishi et al. 1996; Rawlings et al. 2003). Its optical depth $\tau_{3.4}$ is estimated to be 0.17, which corresponds to A_V = 25–40 mag, if the dust extinction curve in NGC 1377 is similar to the Galactic diffuse interstellar medium ($\tau_{3.4}/A_V \sim$ 0.004–0.007; Pendleton et al. 1994).

For Cygnus A ($z = 0.056$) and 3C 234 ($z = 0.185$), the presence of the 3.4 μm absorption feature in our L-band spectra is uncertain. We estimate conservative upper limits of $\tau_{3.4} < 0.2$ for both sources, which corresponds to $A_V < 50$ mag toward the L-band continuum emitting regions, if the Galactic relation of $\tau_{3.4}/A_V \sim$ 0.004–0.007 is assumed. The A_V value derived from our L-band spectra is at the lower end of the range for Cygnus A (A_V =

---

[5] IRAF is a general purpose software system distributed by the National Optical Astronomy Observatories, which are operated by the Association of Universities for Research in Astronomy, Inc. (AURA), under cooperative agreement with the National Science Foundation.

40–150 mag; §2.4) and is smaller than the other estimate for 3C 234 (A_V = 60 mag; §2.4).

4.1.4. *[MgVIII]3.028μm emission*

3C 234 ($z = 0.185$) shows an emission line at $\lambda_{obs} \sim 3.58$ μm or $\lambda_{rest} \sim 3.02$ μm, which we identify as the [Mg VIII] 3.028μm line. We estimate its flux to be f([MgVIII]) = 1.5×10^{-14} ergs s^{-1} cm^{-2}, and its luminosity to be L([MgVIII]) = 1.2×10^{42} ergs s^{-1}.

4.2. *K-band spectra*

For the two sources observed with IRTF SpeX, i.e., IC 860 and CGCG 1510.8+0725 (weak [CII] emitters), *K*-band spectra are obtained simultaneously with the *L*-band spectra. Figure 2 shows these *K*-band spectra.

The spectra of IC 860 (z = 0.013) and CGCG 1510.8+0725 (z = 0.013) show gaps in the continuum at $\lambda_{obs} \sim 2.35$ μm. We attribute these gaps to CO absorption features at λ_{rest} = 2.31–2.4 μm produced by stars (Ivanov et al. 2000; Imanishi & Alonso-Herrero 2004; Imanishi & Wada 2004). For the other weak [CII] emitter, NGC 4418 (Malhotra et al. 1997), the CO absorption feature is clearly detected (Imanishi et al. 2004). To estimate the CO absorption strengths in IC 860 and CGCG 1510.8+0725, we adopt the spectroscopic CO index (CO_{spec}) defined by Doyon et al. (1994) and follow the procedures applied to NGC 4418 (Imanishi et al. 2004). For both IC 860 and CGCG 1510.8+0725, power-law continuum levels ($F_\lambda = \alpha \times \lambda^\beta$) are determined using data points at λ_{obs} = 2.08–2.32 μm (λ_{rest} = 2.05–2.29 μm), excluding obvious emission lines. The adopted continuum levels are shown as dashed lines in Figure 2. Data at λ_{obs} = 2.34–2.43 μm (λ_{rest} = 2.31–2.40 μm) are used to derive the CO_{spec} values. We obtain $CO_{spec} \sim 0.1$ for IC 860 and ∼0.2 for CGCG 1510.8+0725. However, the continuum determination of IC 860 is less secure than CGCG 1510.8+0725 because of the large scatter of continuum data points in the former (Figure 2). We try several continuum levels within a reasonable range, and obtain the largest plausible value of $CO_{spec} \sim 0.2$ for IC 860.

The typical values observed in star-forming or elliptical (=spheroidal) galaxies are $CO_{spec} > 0.15$ (Goldader et al. 1997a,b; Ivanov et al. 2000). Dilution of the CO absorption feature by a featureless continuum from AGN-heated hot dust or from stars younger than a few million years (Leitherer et al. 1999) can decrease the CO_{spec} values. Based on CO_{spec} values, there is no explicit AGN evidence in IC 860 and CGCG 1510.8+0725.

The *K*-band spectrum of CGCG 1510.8+0725 shows strong H_2 emission features, as with NGC 4418 (Imanishi et al. 2004). For NGC 4418, strong H_2 emission lines and other observational properties are naturally explained by a powerful buried AGN (Dudley & Wynn-Williams 1997; Spoon et al. 2001; Imanishi et al. 2004). However, the signal-to-noise ratios for CGCG 1510.8+0725 are not good enough to investigate in a quantitatively detailed manner whether the strong H_2 emission originates in a buried AGN or other mechanisms related to starbursts.

5. DISCUSSION

5.1. *Detected modestly obscured starbursts*

3.3 μm PAH emission, a signature of starbursts, is detected in six of nine observed infrared luminous galaxies. Since dust extinction in the *L*-band is about 0.06 times as large as that in the optical *V*-band (λ = 0.6 μm; Rieke & Lebofsky 1985), the flux of the 3.3 μm PAH emission is not significantly attenuated (<1 mag) if dust extinction is less than 15 mag in A_V. Thus, the observed 3.3 μm PAH emission luminosities are a good measure of the absolute luminosity of modestly obscured (A_V < 15 mag) starburst activity.

Table 3 summarizes the observed 3.3 μm PAH to infrared luminosity ratios ($L_{3.3PAH}/L_{IR}$). The ratios are factors of 3 to >10 lower than those reported for modestly obscured starbursts (∼10^{-3}; Mouri et al. 1990; Imanishi 2002). If these ratios are taken at face value, the detected modestly obscured starbursts can account for only some fraction of the infrared luminosities of these galaxies. The infrared luminosities must therefore be dominated by AGNs and/or very heavily obscured (A_V >> 15 mag) starbursts.

5.2. *AGNs obscured by torus-shaped dust in optical Seyfert 2s*

IRAS 04154+1755, Cygnus A, and 3C 234 are classified optically as Seyfert 2s (Table 1). Their optical Seyfert 2 classifications indicate that (1) the AGNs are obscured along our line of sight by torus-shaped dust, (2) a large amount of the AGNs' ionizing photons are escaping along the torus axis, and (3) emission lines, originating in the well-developed narrow line regions (NLRs), are strong and clearly detectable in the optical spectra. For these optical Seyfert 2s, the presence of obscured AGNs is much more certain than in other infrared luminous galaxies with no optical Seyfert signatures (non-Seyferts). Hence, it is useful to test whether our *L*-band spectroscopic method can succeed in detecting AGN signatures in these optical Seyfert 2s.

For Cygnus A and 3C 234, the 3.3 μm PAH equivalent widths (Table 3) are more than an order of magnitude lower than those of typical starburst galaxies ($EW_{3.3PAH}$ ∼100 nm; Moorwood 1986; Imanishi & Dudley 2000). The observed *L*-band fluxes must be dominated by PAH-free emission, most plausibly a featureless continuum from AGN-heated hot dust. Thus, our *L*-band spectroscopy has successfully revealed AGN signatures in these two optical Seyfert 2s.

For 3C 234, the [Mg VIII]3.028μm emission line is detected. The ionization potential of the [Mg VIII] line is as high as 224.9 eV, and this emission line has been detected in several nearby Seyfert galaxies (Lutz et al. 2000; Sturm et al. 2002; Marco & Brooks 2003). The detection of such a high excitation forbidden emission line requires a very hard radiation field, further supporting the presence of an AGN.

The [Mg VIII] luminosity of 3C 234 is larger than the prototypical nearby Seyfert 2 galaxy NGC 1068 by a factor of 40 (Marco & Brooks 2003). The observed 2–10 keV X-ray luminosity from the AGN in NGC 1068 is estimated to be ∼1×10^{41} ergs s^{-1}, but this is believed to be a reflected component (Koyama et al. 1989). Assuming a reflected fraction of 0.01 (Pier et al. 1994), the intrinsic 2–10 keV luminosity in NGC 1068 is Lx(2–10 keV) ∼ 10^{43} ergs s^{-1}. If the [Mg VIII] to 2–10 keV luminosity ratio in 3C 234 is similar to that of NGC 1068, then the predicted 2–10 keV luminosity for 3C 234 is Lx(2–10 keV) $\sim 4 \times 10^{44}$ ergs s^{-1}, which is roughly comparable to the measured value of $\sim 1 \times 10^{44}$ ergs s^{-1} (Sambruna et al. 1999).

For IRAS 04154+1755, the presence of an AGN is less certain than for Cygnus A and 3C 234, if we consider the $EW_{3.3PAH}$ value (∼60 nm for IRAS 04154+1755; Table 3). However, the relatively large $EW_{3.3PAH}$ value in IRAS 04154+1755 is probably the consequence of the strong ($\tau_{3.1} \sim 0.9$) 3.1 μm H_2O ice absorption. This absorption feature strongly attenuates the AGN-originated flux and reduces the dilution of the 3.3 μm PAH emission by an AGN continuum, making the $EW_{3.3PAH}$ value relatively large, even in the presence of a powerful obscured AGN. We therefore search for signatures of an obscured AGN based on a $\tau_{3.1}$ value.

As mentioned in §1, and in more detail in Imanishi & Maloney (2003) and Imanishi et al. (2006), $\tau_{3.1}$ values can be used to distinguish between a normal starburst (mixed source/dust geometry, small $\tau_{3.1}$) or an obscured AGN (centrally-concentrated energy source geometry, large $\tau_{3.1}$). Since the fraction of dust covered with an ice mantle in the majority of infrared luminous galaxies is likely to be smaller than the well-studied less infrared-luminous starburst galaxy M82, because of harsher radiation environment in the former (Soifer et al. 2000, 2001), $\tau_{3.1}$ larger than 0.3 suggests a centrally-concentrated energy source geometry (Imanishi & Maloney 2003; Imanishi et al. 2006). The large observed $\tau_{3.1}$ of IRAS 04154+1755 (∼0.9) strongly indicates a centrally-concentrated energy source, such as an obscured AGN. We note that IRAS 04154+1755 is located close to the Galactic Taurus molecular clouds, but no significant molecular gas is detected in the exact direction of IRAS 04154+1755 (Ungerechts & Thaddeus 1987). Furthermore, the wavelength range in which H_2O ice absorption is strong in Figure 1 is similar to that expected from the profile of GL 2591 redshifted with $z = 0.056$, rather than $z = 0$. Thus, the strong 3.1 μm H_2O absorption in IRAS 04154+1755 is believed to be nuclear in origin.

In summary, our *L*-band spectroscopic method successfully provides AGN evidence for the three optical Seyfert 2s, which are known to possess luminous AGNs behind torus-shaped dust. Imanishi et al. (2006) also detected AGN signatures in the *L*-band spectra of all observed ultraluminous infrared galaxies classified optically as Seyferts. We can therefore conclude that our *L*-band spectroscopic method is at least as effective as conventional optical spectroscopy for the purpose of finding AGNs obscured behind dust. However, the question of how much more effective our *L*-band method is depends on the detection rate of buried AGNs in optical non-Seyfert galaxies.

5.3. *Buried AGNs in NGC 828 and NGC 1377*

Among the six observed optical non-Seyfert galaxies (NGC 828, IRAS 15250+3609, IRAS 17208−0014, NGC 1377, IC 860, and CGCG 1510.8+0725), the $EW_{3.3PAH}$ values of NGC 828 and NGC 1377 are $\lesssim$ 20 nm. Starburst galaxies have an average value of $EW_{3.3PAH} \sim$ 100 nm, with some scatter, but never lower than ∼40 nm (Moorwood 1986). The small $EW_{3.3PAH}$ values of NGC 828 and NGC 1377 suggest that powerful AGNs are present, which heat up dust grains and produce strong PAH-free featureless continua that dilute the 3.3 μm PAH emission from starbursts. Our *L*-band spectroscopy thus newly reveals buried AGN signatures in two optical non-Seyfert galaxies.

The *L*-band continuum of NGC 1377 is unusually red compared to normal starburst emission. Such red *L*-band continua have previously been observed in the ultraluminous infrared galaxies Superantennae (Risaliti et al. 2003) and IRAS 08572+3915 (Imanishi et al. 2006), both of which show very weak 3.3 μm PAH emission and are therefore classified as obscured-AGN-dominated. Very highly reddened hot dust emission heated by an obscured AGN is the most natural explanation for the extremely red *L*-band continuum of NGC 1377 (Risaliti et al. 2006). The observed $\tau_{3.4}$ value of 0.17 corresponds to A_V = 25–40 mag, or $A_{3.5\mu m}$ = 1.4–2.5 mag if the Galactic dust extinction curve is adopted. Thus, the dereddened luminosity heated by an AGN is $\nu L_\nu(3.8\mu m) = 0.4–1 \times 10^{43}$ ergs s^{-1}, which can account for a significant fraction of the infrared luminosity of NGC 1377 ($L_{IR} \sim 3 \times 10^{43}$ ergs s^{-1}).

5.4. *Weak signatures of buried AGNs in IRAS 17208−0014 and CGCG 1510.8+0725*

For the two optical non-Seyfert galaxies IRAS 17208−0014 and CGCG 1510.8+0725, some indications of buried AGNs might be present.

For IRAS 17208−0014, the large $\tau_{3.1}$ value of ∼0.4 suggests a centrally-concentrated energy source, such as a buried AGN, if the fraction of ice-covered dust is comparable to or smaller than that in the well-studied starburst galaxy M82. However, Soifer et al. (2000) found that the mid-infrared 12.5 μm dust emission from IRAS 17208−0014 is dominated by spatially extended components, with no prominent core, indicating that dust emission at this wavelength is dominated by extended starburst activity. The estimated surface brightness of IRAS 17208−0014 is exceptionally low compared to other ultraluminous infrared galaxies ($L_{IR} > 10^{12} L_\odot$), and can even be smaller than that of M82 (Soifer et al. 2000). Hence, the fraction of ice-covered dust can be larger than that in M82, because of a weaker radiation density in IRAS 17208−0014. Unlike the majority of other infrared luminous galaxies, the observed $\tau_{3.1}$ value of ∼0.4 in IRAS 17208−0014 could be reproduced by a mixed source/dust geometry (§5.2). Millimeter interferometric observations, based on the HCN (J = 1–0) to HCO^+ (J = 1–0) ratio in brightness temperature, have suggested that a buried AGN might be present, but failed to reveal clear AGN evidence (Imanishi et al. 2006). For this source, although absorption features at 5–11.5 μm are found, 6.2 μm PAH emission is also strong (Spoon et al. 2002). The presence of a luminous buried AGN in IRAS 17208−0014 has not been explicitly indicated in any available data and so is currently unclear.

For the weak [CII] emitter CGCG 1510.8+0725, strong H_2 emission might originate in a buried AGN (§4.2), but the buried AGN evidence is not strong. Although the presence of a strong buried AGN is one possibility to explain the small [CII] to far-infrared continuum luminosity ratio (Malhotra et al. 1997, 2001), scenarios that do not invoke a powerful buried AGN, such as large radiation density or optical depth effects in starbursts (Malhotra et al. 1997, 2001), could be alternative possibilities for the weak [CII] emission. It is unclear whether CGCG 1510.8+0725 does in fact possess a luminous buried AGN.

5.5. *No explicit buried AGN signatures in IC 860 and IRAS 15250+3609*

For the remaining two optical non-Seyfert galaxies IC 860 and IRAS 15250+3609, no explicit buried AGN signatures are evident in our spectra. For the weak [CII] emitter IC 860, it is unclear whether there is indeed a powerful buried AGN, as in the case of CGCG 1510.8+0725 (§5.4).

IRAS 15250+3609 shows strong absorption features, with very weak PAH emission in its mid-infrared 5–11.5 μm spectrum. These mid-infrared properties are very similar to NGC 1377, and yet the *L*-band spectra are very different, in that only NGC 1377 shows strong buried AGN signatures. This discrepancy probably derives from the different overall spectral energy distributions. Figure 3 shows infrared 1–11.5 μm spectral energy distributions of NGC 1377 and IRAS 15250+3609. The emission at 5–11.5 μm is dominated by dust emission powered by obscured energy sources (starbursts and/or AGNs), whereas that at 1–2.5 μm originates in foreground stellar emission. The signatures of obscured AGNs can only be detected in the *L*-band spectra if AGN-heated hot dust emission contributes significantly to the observed *L*-band flux.

In Figure 3 (*Left*), the *L*-band emission of NGC 1377 is smoothly connected to the longer wavelength dust emission spectrum observed with *ISO*, which is judged to be powered by an obscured AGN, because of strong absorption and lack of PAH emission features (Laureijs et al. 2000). Detection of strong AGN signatures in the *L*-band spectrum of NGC 1377 is possible primarily because the AGN-heated dust emission is a dominant component at *L*. In contrast, the *L*-band emission of IRAS 15250+3609 (Figure 3, *Right*) corresponds to a transition between stellar and dust emission. The shorter part of the *L*-band spectrum (<3.5 μm) is likely to be dominated by foreground stellar emission, which is why we missed clear AGN signatures in our *L*-band spectrum of IRAS 15250+3609, despite its 5–11.5 μm spectrum strongly suggesting the presence of a powerful obscured AGN.

6. SUMMARY

We reported infrared *L*-band spectroscopic results for nine infrared luminous galaxies that may possess signatures of AGNs hidden behind dust based on observational data at other wavelengths. A radio to far-infrared excess galaxy (IRAS 04154+1755), four sources that exhibit absorption features in the 5–11.5 μm spectra (NGC 828, IRAS 15250+3609, IRAS 17208−0014, and NGC 1377), two weak [CII] 158μm emitters (IC 860 and CGCG 1510.8+0725), and two narrow-line radio galaxies (Cygnus A and 3C 234) were observed. Using the 3.3 μm PAH emission feature, the [Mg VIII] 3.028 μm emission line, and absorption features at 3.1 μm from ice-covered dust and at 3.4 μm from bare carbonaceous dust, we searched for signatures of obscured AGNs in our *L*-band spectra. For the two weak [CII] emitters, *K*-band spectra were also simultaneously taken. We found the following main results:

1. For two optical Seyfert 2 galaxies (Cygnus A and 3C 234), our results strongly suggested that the observed *L*-band spectra are dominated by a PAH-free featureless continuum, originating in AGN-heated hot dust, because of very small 3.3 μm PAH equivalent widths. A strong detection of the [Mg VIII] 3.028 μm line in the *L*-band spectrum of 3C 234 also supported the presence of a luminous AGN behind torus-shaped dust in this source.

2. For another optical Seyfert 2 galaxy, IRAS 04154+1755, an energy source that is more centrally concentrated than dust was suggested from the large optical depth of the 3.1 μm dust absorption feature ($\tau_{3.1} \sim 0.9$). An obscured AGN is a natural explanation for this energy source, because in normal starburst galaxies, stellar energy sources and dust are spatially well mixed.

3. Our *L*-band spectroscopic method succeeded in detecting clear AGN signatures in all three optical Seyfert 2s known to possess powerful AGNs behind torus-shaped dust. This means that as a tool for finding obscured AGNs, our *L*-band spectroscopic method is at least as powerful as conventionally used optical spectroscopy.

4. Among the remaining six optical non-Seyferts (NGC 828, IRAS 15250+3609, IRAS 17208−0014, NGC 1377, IC 860, and CGCG 1510.8+0725), strong AGN signatures were found in NGC 828 and NGC 1377, based on their very small 3.3 μm PAH equivalent widths. NGC 1377 showed a very red *L*-band continuum, which also supports the obscured-AGN-dominated nature of this galaxy. The detection of AGNs in the two optical non-Seyferts clearly indicated that our *L*-band spectroscopic method is more effective than optical spectroscopy in finding obscured AGNs.

5. IRAS 17208−0014 and NGC 1377 may have shown 3.1 μm and 3.4 μm dust absorption features with optical depths of $\tau_{3.1} \sim 0.4$ and $\tau_{3.4} \sim 0.17$, respectively. The large $\tau_{3.1}$ value of IRAS 17208−0014 indicated a centrally-concentrated energy source, such as a buried AGN, if the fraction of ice-covered dust is similar to or smaller than that in the well-studied starburst galaxy M82.

6. Strong H_2 emission found in the *K*-band spectrum of the weak [CII] emitter CGCG 1510.8+0725 might come from phenomena related to a buried AGN, like another weak [CII] emitter NGC 4418.

7. For IRAS 17208−0014 and CGCG 1510.8+0725, possible buried AGNs signatures were found, but weak. For IC 860 and IRAS 15250+3609, we failed to provide any explicit buried AGN evidence in our spectra. The non-detection of buried AGN signatures in IRAS 15250+3609 was explained by its infrared 1–11.5 μm spectral energy distribution, where foreground stellar emission is dominant at *L*. However, for the remaining three optical non-Seyfert galaxies IRAS 17208−0014, IC 860, and

CGCG 1510.8+0725, the evidence for buried AGNs at other wavelengths is also very weak. The absence of buried AGN signatures in these sources may be due to their starburst-dominated nature.

We are grateful to M. Ishii, R. Potter, E. Pickett, A. Hatakeyama, M. Lemmen, B. Golisch, and D. Griep for their support during our Subaru and IRTF observations. We thank the anonymous referee for his/her useful comments. Text data of ISO spectra of IRAS 15250+3609 and NGC 1377 were kindly provided by H. W. W. Spoon. M.I. is supported by Grants-in-Aid for Scientific Research (16740117). Some of the data analysis was carried out using a computer system operated by the Astronomical Data Analysis Center (ADAC) and the Subaru Telescope of the National Astronomical Observatory, Japan. This research has made use of the SIMBAD database, operated by the Centre de Donnees astronomiques de Strasbourg (CDS), Strasbourg, France; of the NASA/IPAC Extragalactic Database (NED), which is operated by the Jet Propulsion Laboratory, California Institute of Technology, under contract with the National Aeronautics and Space Administration (NASA); and of data products from the Two Micron All Sky Survey, which is a joint project between the University of Massachusetts and the Infrared Processing and Analysis Center/California Institute of Technology, funded by NASA and the National Science Foundation.

REFERENCES

Antonucci, R. 1993, ARA&A, 31, 473
Antonucci, R., & Barvainis, R. 1990, ApJ, 363, L17
Barger, A. J., Cowie, L. L., & Richards, E. A. 2000, AJ, 119, 2092
Condon, J. J., Anderson, M. L., & Helou, G. 1991, ApJ, 376, 95
Crawford, T., Marr, J., Partridge, B., & Strauss, M. M. 1996, ApJ, 460, 225
Djorgovski, S., Weir, N., Matthews, K., & Graham, J. R. 1991, ApJ, 372, L67
Doyon, R., Joseph, R. D., & Wright, G. S. 1994, ApJ, 421, 101
Draine, B. T., & Lee, H. M. 1984, ApJ, 285, 89
Dudley, C. C., & Wynn-Williams, C. G. 1997, ApJ, 488, 720
Fabian, A. C., Wilman, R. J., & Crawford, C. S., 2002, MNRAS, 329, L18
Forster Schreiber, N. M., Genzel, R., Lutz, D., Kunze, D., & Sternberg, A. 2001, ApJ, 552, 544
Genzel, R. et al. 1998, ApJ, 498, 579
Goldader, J. D., Joseph, R. D., Doyon, R., & Sanders, D. B. 1997a, ApJ, 474, 104
Goldader, J. D., Joseph, R. D., Doyon, R., & Sanders, D. B. 1997b, ApJS, 108, 449
Grandi, S. A., & Osterbrock, D. E. 1978, ApJ, 220, 783
Imanishi, M. 2000a, MNRAS, 313, 165
Imanishi, M. 2000b, MNRAS, 319, 331
Imanishi, M. 2002, ApJ, 569, 44
Imanishi, M., & Alonso-Herrero, A. 2004, ApJ, 614, 122
Imanishi, M., & Dudley, C. C. 2000, ApJ, 545, 701
Imanishi, M., & Maloney, P. R. 2003, ApJ, 588, 165
Imanishi, M., & Ueno, S., 1999, ApJ, 527, 709
Imanishi, M., & Ueno, S., 2000, ApJ, 535, 626
Imanishi, M., & Wada, K., 2004, ApJ, 617, 214
Imanishi, M., Dudley, C. C., & Maloney, P. R. 2001, ApJ, 558, L93
Imanishi, M., Dudley, C. C., & Maloney, P. R. 2006, ApJ, 637, 114 (astro-ph/0509861)
Imanishi, M., Nakanishi, K., Kuno, N., & Kohno, K., 2004, AJ, 128, 2037
Imanishi, M., Nakanishi, K., & Kohno, K. 2006, AJ, in press (astro-ph/0602227)
Imanishi, M., Sasaki, Y., Goto, M., Kobayashi, N., Nagata, T., & Jones, T. J. 1996, AJ, 112, 235
Ivanov, V. D., Rieke, G. H., Groppi, C. E., Alonso-Herrero, A., Rieke, M. J., & Engelbracht, C. W. 2000, ApJ, 545, 190
Iye, M., Karoji, H., Ando, H., Kaifu, N., Kodaira, K., Aoki, K., Aoki, W., Chikada, Y., et al. 2004, PASJ, 56, 381
Kim, D. -C., & Sanders, D. B., 1998, ApJS, 119, 41
Kobayashi, N., et al. 2000, IRCS: Infrared camera and spectrograph for the Subaru Telescope, in Proc. SPIE 4008: Optical and IR Telescope Instrumentation and Detectors, eds M. Iye & A. F. Moorwood, 1056
Koyama, K., Inoue, H., Tanaka, Y., Awaki, H., Takano, S., Ohashi, T., & Matsuoka, M. 1989, PASJ, 41, 731
Laureijs, R. J., et al. 2000, A&A, 359, 900
Leitherer, C. et al. 1999, ApJS, 123, 3
Lutz, D. et al. 1996, A&A, 315, L269
Lutz, D., Sturm, E., Genzel, R., Moorwood, A. F. M., Alexander, T., Netzer, H., & Sternberg, A. 2000, ApJ, 536, 697
Maiolino, R. et al. 2003, MNRAS, 344, L59
Malhotra, S. et al. 1997, ApJ, 491, L27
Malhotra, S. et al. 2001, ApJ, 561, 766
Maloney, P., Hollenbach, D., & Tielens, A. G. G. M. 1996, ApJ, 466, 561
Marco, O., & Brooks, K. J. 2003, A&A, 398, 101
Mathis, J. S., & Whiffen, G. 1989, ApJ, 341, 808
McLeod, K. K., Rieke, G. H., Rieke, M. J., & Kelly, D. M. 1993, ApJ, 412, 111
Moorwood, A. F. M. 1986, A&A, 166, 4
Mouri, H., Kawara, K., Taniguchi, Y., & Nishida, M. 1990, ApJ, 356, L39
Murakawa, K., Tamura, M., & Nagata, T. 2000, ApJS, 128, 603
Murphy, Jr, T. W., Soifer, B. T., Matthews, K., Armus, L., & Kiger, J. R. 2001, AJ, 121, 97
Osterbrock, D. E., & Miller, J. S. 1975, ApJ, 197, 535
Packham, C., Young, S., Hough, J. H., Tadhunter, C. N., & Axon, D. J. 1998, MNRAS, 297, 936
Pendleton, Y. J., Sandford, S. A., Allamandola, L. J., Tielens, A. G. G. M., & Sellgren, K. 1994, ApJ, 437, 683
Pier, E. A., Antonucci, R., Hurt, T., Kriss, G., & Krolik, J. 1994, ApJ, 428, 124
Puxley, P. J. 1991, MNRAS, 249, 11p
Rawlings, M. G., Adamson, A. J., & Whittet, D. C. B. 2003, MNRAS, 341, 1121
Rayner, J. T., Toomey, D. W., Onaka, P. M., Denault, A. J., Stahlberger, W. E., Vacca, W. D., Cushing, M. C., & Wang, S. 2003, PASP, 115, 362
Rieke, G. H., & Lebofsky, M. J. 1985, ApJ, 288, 618
Risaliti, G., et al. 2003, ApJ, 595, L17
Risaliti, G., et al. 2006, MNRAS, 365, 303
Robson, I. 1996, Active Galactic Nuclei (New York: Wiley)
Sambruna, R. M., Eracleous, M., & Mushotzky, R. F. 1999, ApJ, 526, 60
Sanders, D. B., & Mirabel, I. F. 1996, ARA&A, 34, 749
Sanders, D. B., Soifer, B. T., Elias, J. H., Neugebauer, G., & Matthews, K. 1988, ApJ, 328, L35
Siebenmorgen, R., Krugel, E., & Spoon, H. W. W. 2004, A&A, 414, 123
Smith, R. G., Sellgren, K., & Tokunaga, A. T. 1989, ApJ, 344, 413
Smith, R. G., Sellgren, K., & Brooke, T. Y. 1993, MNRAS, 263, 749
Soifer, B. T., Sanders, D. B., Madore, B. F., Neugebauer, G., Danielson, G. E., Elias, J. H., Lonsdale, C. J., & Rice, W. L. 1987, ApJ, 320, 238
Soifer, B. T. et al. 2000, AJ, 119, 509
Soifer, B. T. et al. 2001, AJ, 122, 1213
Spoon, H. W. W., Koornneef, J., Moorwood, A. F. M., Lutz, D., & Tielens, A. G. G. M. 2000, A&A, 357, 898
Spoon, H. W. W., Keane, J. V., Tielens, A. G. G. M., Lutz, D., & Moorwood, A. F. M. 2001, A&A, 365, L353
Spoon, H. W. W., Keane, J. V., Tielens, A. G. G. M., Lutz D Moorwood, A. F. M., & Laurent, O. 2002, A&A, 385, 102
Spoon, H. W. W., Moorwood, A. F. M., Lutz, D., Tielens, A. G. G. M., Siebenmorgen, R., & Keane, J. V. 2004, A&A, 414, 873
Sturm, E., Lutz, D., Tran, D., Feuchtgruber, H., Genzel, R., Kunze, D., Moorwood, A. F. M., & Thornley, M. D. 2000, A&A, 358, 481

Sturm, E., Lutz, D., Verma, A., Netzer, H., Sternberg, A., Moorwood, A. F. M., Oliva, E., & Genzel, R. 2002, A&A, 393, 821

Tadhunter, C. N. et al. 1999, ApJ, 512, L91

Tanaka, M., Sato, S., Nagata, T., & Yamamoto, T. 1990, ApJ, 352, 724

Tokunaga A. T., Sellgren K., Smith R. G., Nagata T., Sakata A., Nakada Y., 1991, ApJ, 380, 452

Tokunaga, A. T. 2000, in Allen's Astrophysical Quantities, ed. A. N. Cox (4th ed; Berlin: Springer), 143

Ueno, S., Koyama, K., Nishida, M., Yamauchi, S., & Ward, M. J. 1994, ApJ, 431, L1

Ungerechts, H., & Thaddeus, P. 1987, ApJS, 63, 645

Urry, C. M., & Padovani, P. 1995, PASP, 107, 803

Veilleux, S., & Osterbrock, D. E. 1987, ApJS, 63, 295

Veilleux, S., Kim, D. -C., Sanders, D. B., Mazzarella, J. M., & Soifer, B. T. 1995, ApJS, 98, 171

Veilleux, S., Sanders, D. B., & Kim, D. -C. 1999, ApJ, 522, 139

Voit, G. M. 1992, MNRAS, 258, 841

Ward, M. J. 1996, in Cygnus A - Study of a Radio Galaxy, Carilli, C. L., & Harris, D. E., eds, Cambridge University Press, p.43

Whittet, D. C. B., Bode, M. F., Longmore, A. J., Adamson, A. J., McFadzean, A. D., Aitken, D. K., & Roche, P. F. 1988, MNRAS, 233, 321

Wu, H., Zou, Z. L., Xia, X. Y., & Deng, Z. G. 1998, A&AS, 132, 181

Young, S., Axon, D. J., Hough, J. H., Fabian, A. C., & Ward, M. J. 1998, MNRAS, 294, 478

Young, A. J., Wilson, A. S., Terashima, Y., Arnaud, K. A., & Smith, D. A. 2002, ApJ, 564, 176

TABLE 1
INFRARED EMISSION PROPERTIES OF THE OBSERVED INFRARED LUMINOUS GALAXIES

Object (1)	Redshift (2)	f_{12} (Jy) (3)	f_{25} (Jy) (4)	f_{60} (Jy) (5)	f_{100} (Jy) (6)	log $L_{\rm IR}$ (log $L_{\rm IR}/L_{\odot}$) (ergs s^{-1}) (7)	f_{25}/f_{60} (8)	Optical Class (9)
IRAS 04154+1755	0.056	0.20	0.71	3.82	5.84	45.4 (11.8)	0.19 (C)	Sy2 (i)
NGC 828	0.018	0.70	1.03	10.9	22.8	44.9 (11.3)	0.09 (C)	HII (ii)
IRAS 15250+3609	0.055	<0.20	1.32	7.29	5.91	45.6 (12.0)	0.18 (C)	LINER (iii)
IRAS 17208−0014	0.042	0.20	1.66	31.1	34.9	45.9 (12.3)	0.05 (C)	HII (iii)
NGC 1377 (IRAS 03344−2103)	0.005	0.44	1.81	7.25	5.74	43.5 (10.0) [a]	0.25 (W)	unknown (iii)
IC 860 (IRAS 13126+2452)	0.013	<0.09	1.27	17.9	18.1	44.6 (11.0)	0.07 (C)	unknown (iii)
CGCG 1510.8+0725 (Zw 049.057)	0.013	<0.09	0.77	20.8	29.4	44.7 (11.1)	0.04 (C)	HII (iii)
Cygnus A	0.056	<0.25	1.06	2.33	<8.28	45.1–45.4 (11.6–11.9)	0.46 (W)	Sy2 (iv)
3C 234	0.185	0.16	0.26	0.23	<0.35	45.8 (12.2)	1.12 (W)	Sy2 [b] (v,vi,vii)

NOTE. — Col.(1): Object. Col.(2): Redshift. Col.(3)–(6): f_{12}, f_{25}, f_{60}, and f_{100} are *IRAS FSC* fluxes at 12, 25, 60, and 100 μm, respectively. Col.(7): Decimal logarithm of infrared (8–1000 μm) luminosity in ergs s^{-1} calculated with $L_{\rm IR} = 2.1 \times 10^{39} \times$ D(Mpc)^2 $\times$ ($13.48 \times f_{12} + 5.16 \times f_{25} + 2.58 \times f_{60} + f_{100}$) ergs s^{-1} (Sanders & Mirabel 1996). The values in parentheses are the decimal logarithms of the infrared luminosities in units of solar luminosities. Col.(8): *IRAS* 25 μm to 60 μm flux ratio (f_{25}/f_{60}). Galaxies with $f_{25}/f_{60} < 0.2$ and > 0.2 are classified as cool and warm (denoted as "C" and "W"), respectively (Sanders et al. 1988). Col.(9): Optical spectral classification and references. (i): Crawford et al. (1996). (ii): Wu et al. (1998). (iii): Veilleux et al. (1995). (iv): Osterbrock & Miller (1975). (v): Grandi & Osterbrock (1978). (vi): Antonucci & Barvainis (1990). (vii): Young et al. (1998).

[a] The infrared luminosity of NGC 1377 is lower than $L_{\rm IR} \sim 10^{11} L_{\odot}$, but this source is included because there is a strong buried AGN signature (§ 2.2).

[b] 3C 234 shows a broad component of optical Hα emission (Grandi & Osterbrock 1978), but it is more likely to be a scattered component than a direct component (Antonucci & Barvainis 1990; Young et al. 1998). We optically classify this source as a Seyfert 2.

TABLE 2
OBSERVING LOG

Object	Date	Telescope	Integration	P.A.	Standard Stars			
	(UT)	Instrument	(Min)	(°)	Name	L-mag	Type	$T_{\rm eff}$ (K)
(1)	(2)	(3)	(4)	(5)	(6)	(7)	(8)	(9)
IRAS 04154+1755	2005 February 21	Subaru IRCS	32	0	HR 1061	5.1	A0V	9480
NGC 828	2005 February 22	Subaru IRCS	24	0	HR 761	4.9	F8V	6000
IRAS 15250+3609	2005 February 20	Subaru IRCS	16	0	HR 5630	5.0	F8V	6000
IRAS 17208−0014	2005 February 21	Subaru IRCS	24	0	HR 6439	4.4	G9V	5400
NGC 1377	2005 February 20	Subaru IRCS	32	0	HR 1532	4.0	G2.5V	5800
IC 860	2005 April 28	IRTF SpeX	92	0	HR 4864	4.5	G7V	5400
CGCG 1510.8+0725	2005 April 30	IRTF SpeX	100	0	HR 5567	5.8	A0V	9480
Cygnus A	2005 May 29	Subaru IRCS	24	0	HR 7504	4.7	G2.5V	5800
3C 234	2005 February 23	Subaru IRCS	24	0	HR 3815	3.6	G8V	5400

NOTE. — Column (1): Object name. Col. (2): Observing date in UT. Col. (3): Telescope and instrument. Col. (4): Net on-source integration time in min. Col. (5): Position angle of the slit. P.A.(Position angle) = 0° corresponds to the north-south direction. Col. (6): Standard star name. Col. (7): Adopted L-band magnitude. Col. (8): Stellar spectral type. Col. (9): Effective temperature.

TABLE 3
PROPERTIES OF THE 3.3 μM PAH EMISSION

Object (1)	$f_{3.3PAH}$ ($\times 10^{-14}$ ergs s^{-1} cm^{-2}) (2)	$L_{3.3PAH}$ ($\times 10^{41}$ergs s^{-1}) (3)	$L_{3.3PAH}/L_{IR}$ ($\times 10^{-3}$) (4)	rest $EW_{3.3PAH}$ (nm) (5)
IRAS 04154+1755	8.0	5.0	0.2	60
NGC 828	2.0 [a]	0.10	0.02	20
IRAS 15250+3609	5.5	3.5	0.09	110
IRAS 17208−0014	9.0	3.0	0.04	80 [b]
NGC 1377	<1.1 [c]	<0.005	<0.02	<6
IC 860	3.5	0.10	0.03	40
CGCG 1510.8+0725	7.8	0.25	0.05	110
Cygnus A	<0.60	<0.4	<0.03	<6
3C 234	<2.5	<20	<0.3	<4

NOTE. — Col.(1): Object name. Col.(2): Observed flux of the 3.3 μm PAH emission. Col.(3): Observed luminosity of the 3.3 μm PAH emission. Col.(4): Observed 3.3 μm PAH-to-infrared luminosity ratio. Col.(5): Rest-frame equivalent width of the 3.3 μm PAH emission. Starbursts have EW∼100 nm (see text).

[a] The observed PAH profile in this source is slightly wider than the adopted template spectral shape. However, the resulting uncertainty of the PAH flux is insignificant. We employ the same spectral template as other sources for consistency.

[b] This value is similar to that recently estimated by Risaliti et al. (2006) using independent data.

[c] The estimated upper limit is a conservative one, by assuming the lowest plausible continuum level. However, we interpret that an apparent excess at $\lambda_{\rm rest} \sim 3.3$ μm is mostly ascribed to the artifact of the 3.4 μm bare carbonaceous dust absorption feature located at the longer wavelength side.

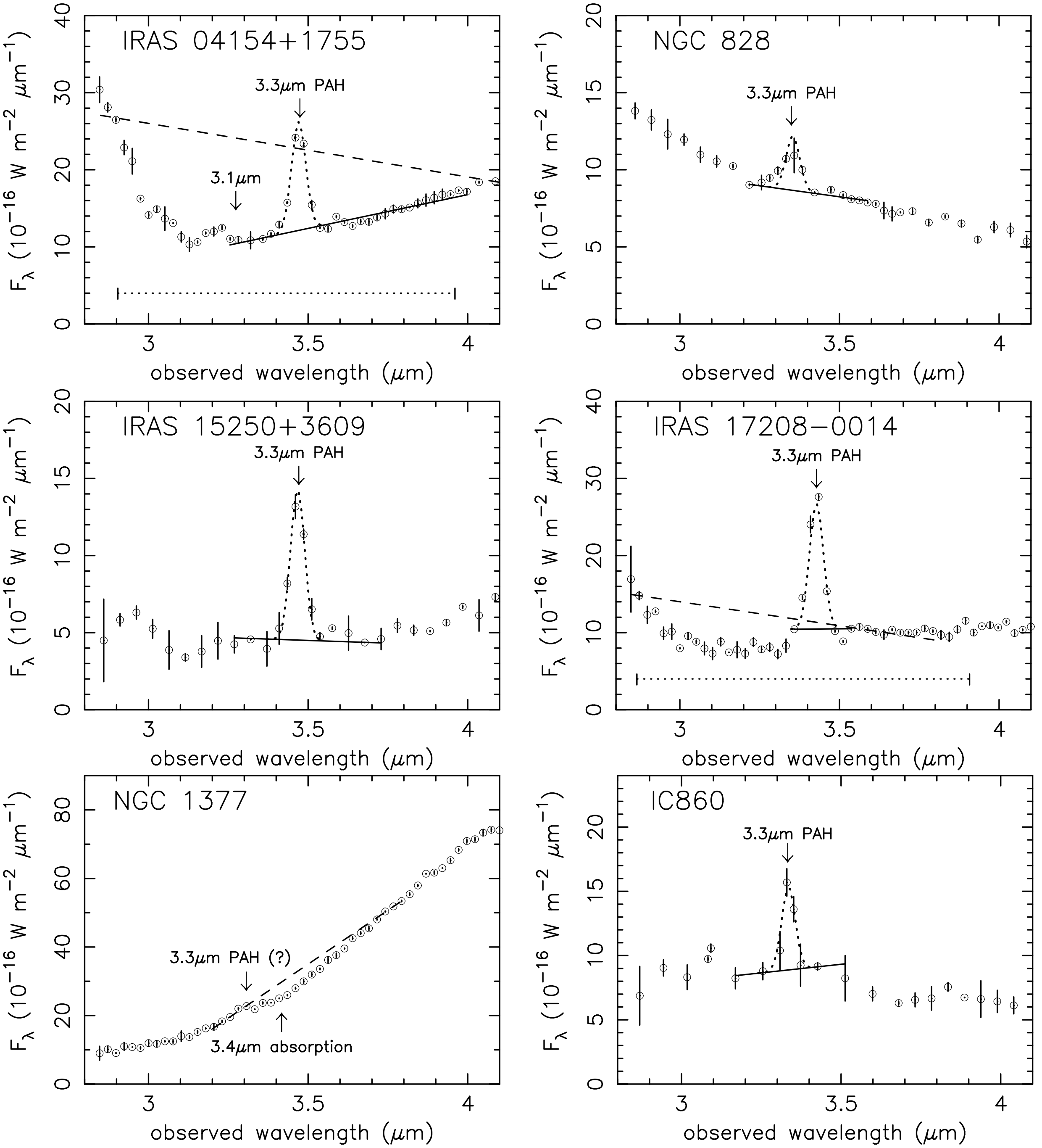
IRAS 04154+1755
3.3μm PAH
3.1μm
NGC 828
3.3μm PAH
IRAS 15250+3609
3.3μm PAH
IRAS 17208−0014
3.3μm PAH
NGC 1377
3.3μm PAH (?)
3.4μm absorption
IC860
3.3μm PAH
F_λ (10^−16 W m^−2 μm^−1)
observed wavelength (μm)
0
5
10
15
20
25
30
35
40
60
80
3
3.5
4

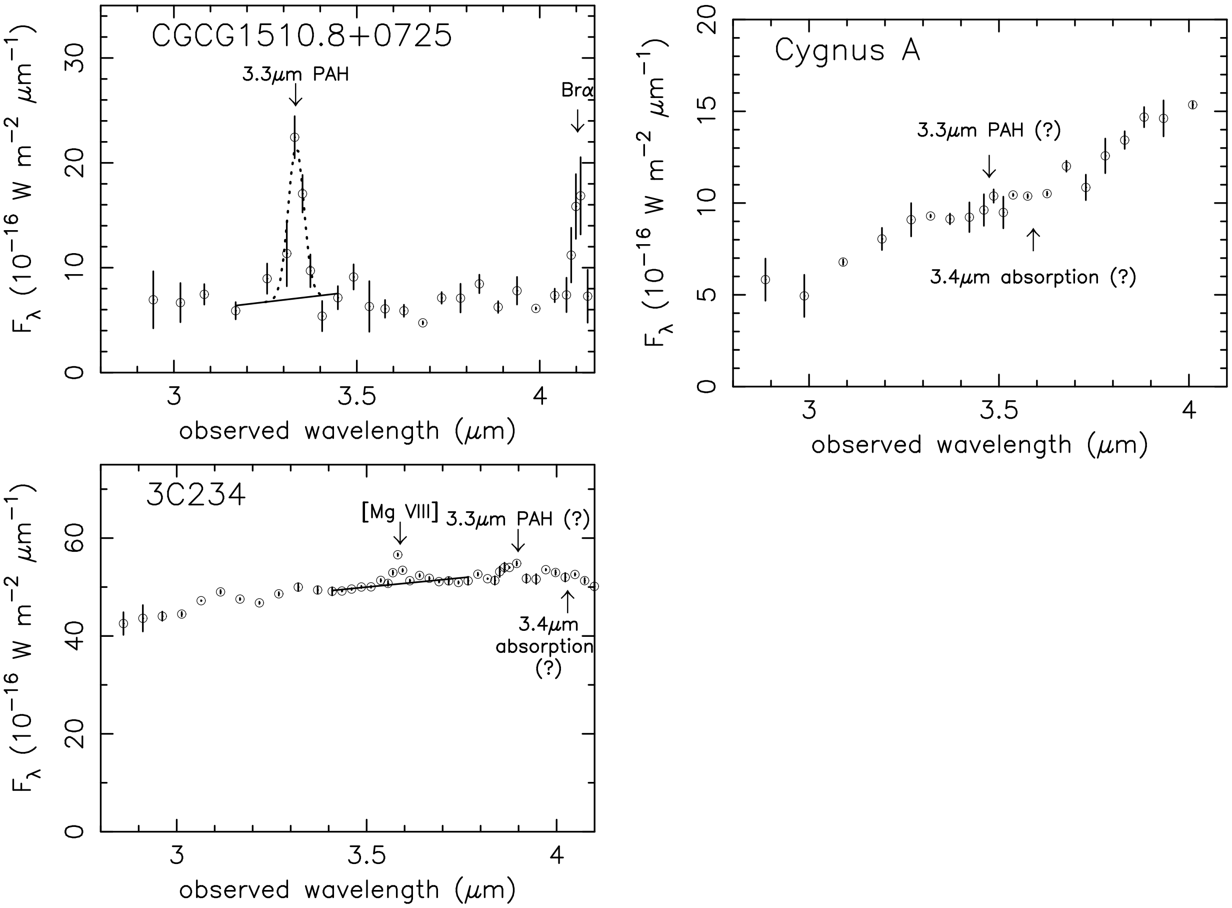

FIG. 1.— Infrared *L*-band (2.8–4.1 μm) spectra of the observed nine infrared luminous galaxies. The abscissa and ordinate are the observed wavelength in μm and flux F_λ in 10^{-16} W m^{-2} μm^{-1}, respectively. For CGCG 1510.8+0725, the spectrum up to $\lambda_{\rm obs}$ = 4.15 μm is presented to show the detected strong Brα emission line. For sources with clearly detectable PAH emission, dotted lines indicate the fittings of the PAH emission, using the template profile (§ 4.1.1), and solid lines are the adopted continuum levels to estimate 3.3 μm PAH fluxes. The dashed lines in the IRAS 04154+1755, IRAS 17208−0014, and NGC 1377 spectra are adopted continuum levels, which are used to measure the optical depths of 3.1 μm ice-covered (IRAS 04154+1755 and IRAS 17208−0014) or 3.4 μm bare carbonaceous dust absorption features (NGC 1377). In the 3C 234 spectrum, the continuum level used to measure the [MgVIII] line flux is shown as a solid line. The horizontal dotted straight lines, inserted between the two short vertical solid lines, at the lower part of the spectra of IRAS 04154+1755 and IRAS 17208−0014 indicate the wavelength range where the effects of the broad 3.1 μm ice absorption feature can be significant ($\lambda_{\rm rest}$ = 2.75–3.75 μm adopted from the spectrum of GL 2591; Smith et al. 1989).

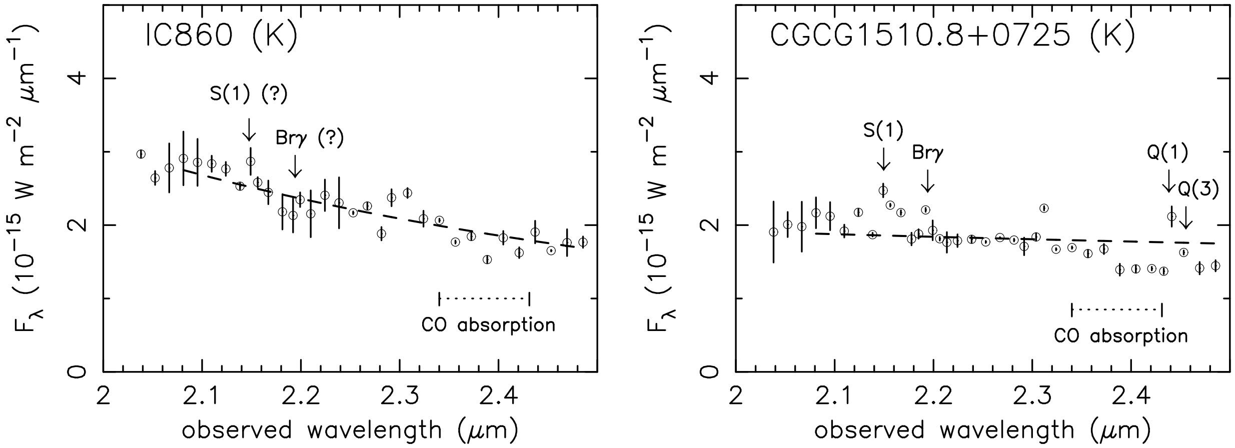

FIG. 2.— Infrared *K*-band (2.0–2.5 μm) spectra of two sources observed with IRTF SpeX (IC 860 and CGCG 1510.8+0725). The abscissa and ordinate are the observed wavelength in μm and flux F_λ in 10^{-15} W m^{-2} μm^{-1}, respectively. The dotted lines inserted between the two vertical lines indicate the wavelength range of the CO absorption feature at $\lambda_{\rm rest}$ = 2.31–2.40 μm. The dashed lines are the continuum levels adopted to measure the strengths of the CO absorption feature. Some detected emission lines are indicated. S(1): H_2 1–0 S(1) at $\lambda_{\rm rest}$ = 2.122 μm. Q(1): H_2 1–0 Q(1) at $\lambda_{\rm rest}$ = 2.407 μm. Q(3): H_2 1–0 Q(3) at $\lambda_{\rm rest}$ = 2.424 μm. Brγ: Brγ emission line at $\lambda_{\rm rest}$ = 2.166 μm.

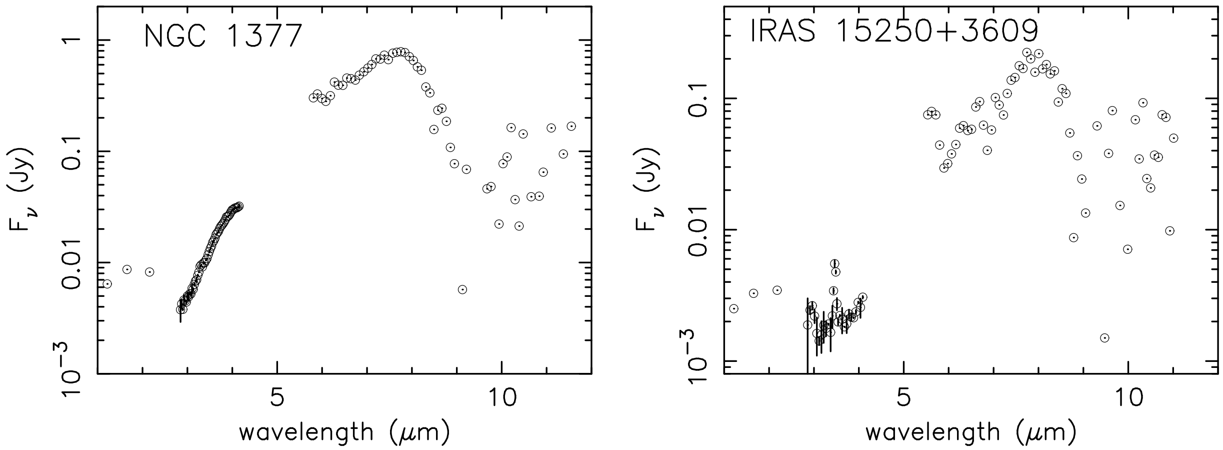

FIG. 3.— Infrared 1–11.5 μm spectral energy distributions of NGC 1377 (*Left*) and IRAS 15250+3609 (*Right*). The abscissa and ordinate are the observed wavelength in μm and flux F_ν in Jy, respectively. Both sources show absorption-dominated 5–11.5 μm mid-infrared spectra, with very weak PAH emission, but the *L*-band spectral shapes are substantially different. Data points are from 2MASS (1–2.5 μm), our *L*-band spectra (2.8–4.1 μm), and *ISO* spectra (5–11.5 μm).